Article

Hollow Multishelled Structural Li-rich Cathode with Al Doping Enabling Capacity and Voltage Stabled Li-ion Batteries

ZHAO Xiaolang[1,2], YANG Mei[1]✉, WANG Jiangyan[1,3]✉ and WANG Dan[1,2,3]✉

Received May 17, 2023
Accepted June 25, 2023

Li-rich layered oxide cathode materials have drawn great attention due to their high specific capacity and relatively low cost. However, their implementation is hindered by capacity and discharge voltage decay as well as poor rate performance. Herein, by combining the concepts of geometrical and atomic structure design, hollow multishelled structural Li-rich cathode material doped with aluminum element(Li-rich HoMS-Al) is developed to solve the above challenges. Li-rich HoMS-Al is synthesized through a facile sequential templating approach with the shell number, element molar ratio and Al doping amount accurately controlled. HoMS can effectively buffer the stress/strain during cycling, as well as shorten the ion and electron diffusion path, while Al doping can inhibit the phase transition of the material and reduce the surface oxygen precipitation. As a result, it achieved a high specific capacity, stable voltage and capacity during cycling, exhibiting an initial discharge specific capacity up to 300.6 mA·h·g^{-1} at 0.1 C(1 C=300 mA/g) and maintaining 246.3 mA·h·g^{-1} after 100 cycles.

Keywords Li-rich layered oxide; Hollow multishelled structure; Aluminum doping; Specific capacity; Cycling stability

1 Introduction

Lithium-ion batteries(LIBs) have been widely used in various fields. In recent years, because of the ever-growing demand for higher energy density and lower cost to further widen the application area of LIBs, diverse electrode materials have been investigated[1−5]. Among emerging electrode materials, Li-rich layered oxide cathode material Li[Li$_x$(MnM)$_{1-x}$]O$_2$(M=Ni, Co, Fe, etc.)(named as LRLO) due to its high specific discharge capacity(>280 mA·h·g^{-1}), high energy density(1000 W·h·L^{-1}) as well as relatively environmental-friendly and low cost has received increasing attention. Its high specific capacity could be achieved after being activated by charging to higher than 4.5 V in the 1st cycle[6−8]. However, this activation process involves irreversible Li$^+$ extraction and oxygen release on the surface, which would induce the layered structure to transform to a spinel structure and transition metal aggregation. Additionally, LRLO suffers from intrinsic poor electron conductivity and lithium ion diffusion kinetics. As a result, problems, such as capacity and discharge voltage decay, low initial Coulombic efficiency and poor rate performance severely hinder its commercialization process[9,10].

Various strategies have been adopted to solve the above challenges, mainly including element doping, nano structuring, etc. Element doping can improve both the surface and bulk structure stability. Many kinds of elements have been investigated to dope into LRLO, including alkali metal cations (Na$^+$, K$^+$)[11,12], alkaline earth metal cations(Mg^{2+}, etc.)[13], transition metal cations(Al^{3+}, Ti^{4+}, Nb^{5+}, etc.)[14−16], anions(F$^-$, Cl$^-$, etc.)[17,18] and polyanions(PO^{3-}, SiO^{4-}, BO^{5-}, etc.)[19,20]. For example, it was found that Al^{3+} can inhibit the spinel phase transition, which significantly improves the capacity retention.

Nano structuring has also been proved to be powerful in improving the performance of LRLO by improving the stress-toleration, shortening the charge diffusion path and inhibiting phase separation[21]. However, over-large specific surface area of nano particles induces severe side reactions and oxygen release, which harms the Coulombic efficiency and cycling life[22]. Given that, hierarchical architectures, which could integrate the strain-toleration and shortened charge diffusion path of nanosized particle units and the reinforced structural stability of secondary assemblies have been intensively developed[23−25].

Among various hierarchical architectures, hollow multishelled structure(HoMS) has been proved to be rather effective in improving the cycling stability and rate capability of rechargeable batteries[26−28]. HoMS is a multi-interface and multi-dimensional micro-nano-scale assembly, which possesses ordered multiple shells(≥2) constructed from nanoparticle units and interconnected cavities[29−32]. HoMS electrode materials offer abundant merits, including: firstly, its internal voids buffers the volume expansion and alleviates the structure strain, thus improving the cycling stability; secondly,

✉ WANG Dan
danwang@ipe.ac.cn
✉ WANG Jiangyan
jywang@ipe.ac.cn
✉ YANG Mei
myang@ipe.ac.cn
1. State Key Laboratory of Biochemical Engineering, Institute of Process Engineering, Chinese Academy of Sciences, Beijing 100190, P. R. China;
2. Qingdao University of Science and Technology, College of Chemistry and Molecular Engineering, Qingdao 266061, P. R. China;
3. School of Chemical Engineering, University of Chinese Academy of Sciences, Beijing 100049, P. R. China

it shortens the charge and ion diffusion distance, and enables a parallel charge diffusion, which results in an enhanced rate capability; more interestingly, compared to single-shelled hollow structure, it offers a larger volumetric capacity and better mechanical and electrochemical stability[33—36]. As a result, a wide variety of HoMS electrode materials have been investigated for energy-related technologies, like rechargeable metal-ion batteries[37], supercapacitors[38], dye-sensitized solar cells[39] and electrocatalysis[40]. However, due to the complex chemical composition of LRLO, the current synthesis of LRLO HoMS materials still suffers from poor atomic level metal cation uniformity.

Wang's group[41—43] developed a sequential templating approach(STA) for HoMS synthesis, which significantly boosts the structural and functional diversity of HoMSs. In this paper, based on STA, Al doped LRLO HoMSs with accurately controlled atomic structure and geometric structure are developed.

2 Experimental

As shown in Fig.1, template with metal ion precursor was synthesized *via* a spray drying process, then LRLO HoMS is obtained *via* a subsequent calcination treatment. By tuning the metal ion concentration and ethylene glycol adding amount, single-shelled(1s), double-shelled(2s), triple-shelled(3s), quadruple-shelled(4s) $Li_{1.2}Mn_{0.54}Ni_{0.13}Co_{0.13}O_2$ hollow spheres and nanoparticles are achieved. In addition, aluminum doping modification was carried out on LRLO 4s HoMS. The results show that Al doped LRLO 4s HoMS exhibits improved electrochemical performance in terms of high specific capacity and enhanced cycling stability, and the discharge specific capacity of HoMSs-$Al_{0.1}$ remains at 246.3 $mA{\cdot}h{\cdot}g^{-1}$ after 100 cycles.

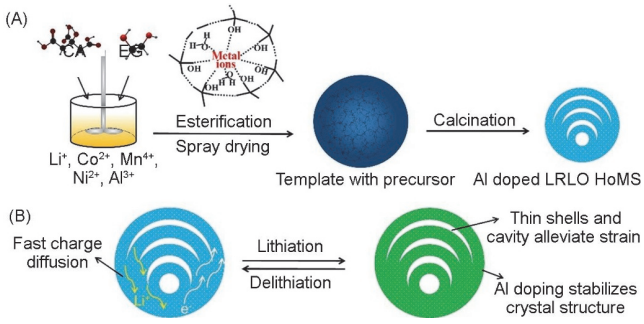

Fig.1 Scheme showing the synthesis process of Al doped LRLO HoMS materials(A) and scheme showing the merits of Al doped LRLO HoMS as cathode materials for LIBs

3 Results and Discussion

3.1 Synthesis of LRLO HoMSs

LRLO HoMSs were synthesized through STA. Firstly, smooth spherical templates with metal ion precursors based on stoichiometric ratio of $Li_{1.2}Mn_{0.54}Ni_{0.13}Co_{0.13}O_2$ or $Li_{1.2}Mn_{0.44}Ni_{0.13}Co_{0.13}Al_{0.1}O_2$(for the doped 4s HoMS, named as 4s HoMS-$Al_{0.1}$) were prepared through a spray drying process (Fig.S1, see the Electronic Supplementary Material of this paper). Then, after a calcination treatment in air, 1s hollow sphere(1s HS), 2s HoMS, 3s HoMS, 4s HoMS, and 4s HoMS-$Al_{0.1}$ LRLO were obtained.

3.2 Characterization of LRLO HoMSs

3.2.1 TGA-DSC

TGA-DSC analysis was carried out to find out the suitable calcination conditions. The mass loss reached 84% with several exothermic peaks observed(Fig.S2, see the Electronic Supplementary Material of this paper) due to the decomposition of the metal ion precursor and the combustion of the template, as well as the crystallization of metal oxide. In the subsequent process above 500 °C, the mass becomes barely changed, which corresponds to the stage of metal ion reorganization to reach the target product with an ideal layered structure.

3.2.2 TEM and HRTEM

TEM images show that the as-prepared LRLO sample is spherical with the hollow multishelled inner structure clearly observed[Fig.2(A)—(C), Fig.S3, see the Electronic Supplementary Material of this paper]. SEM images show that the surface of the synthesized samples is relatively smooth (Fig.S4, see the Electronic Supplementary Material of this paper), the particle size is nonuniform, which is due to that the template is nonuniform. The nonuniform particle may help to increase the packed density of the electrode since the small particles could fill the stacking holes of the big ones. It's worth noting that Al-doped material still maintains a quadruple-shelled structure and a similar size, indicating that Al-doping does not change the morphology. For comparison, LRLO nanoparticles were also prepared(Fig.S5, see the Electronic Supplementary Material of this paper).

In order to distinguish the chemical composition of different samples, inductively coupled plasma emission spectrometer was used to analyze different samples. As shown in Table S1(see the Electronic Supplementary Material of this paper), the detected contents of elements Li, Mn, Ni, Co and Al are basically consistent with their originally designed ratios.

High resolution TEM(HRTEM) shows clear lattice fringes, indicating that the material has good crystallinity, with an interplanar spacing of about 0.46 nm observed for doped and

https://doi.org/10.1007/s40242-023-3128-8

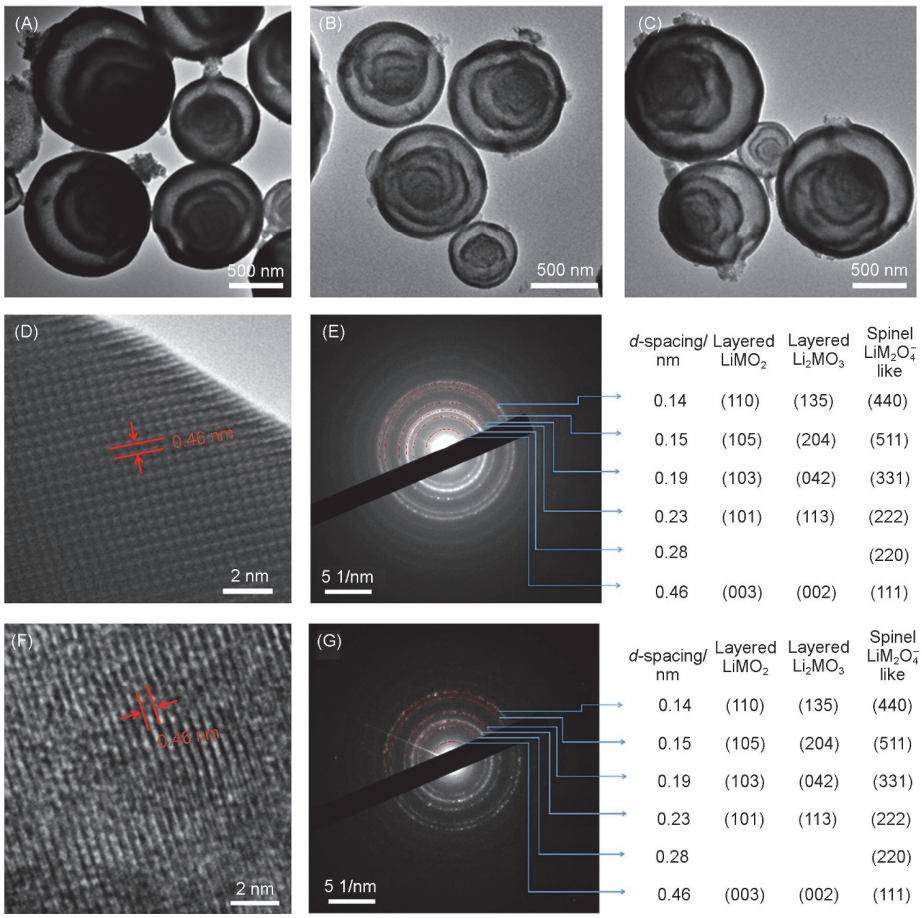

Fig.2 TEM images of 3s HoMS(A), 4s HoMSs(B), 4s HoMSs-Al$_{0.1}$(C), and HRTEM images(D, F) and selected area electron diffraction patterns(E, G) of 4s HoMSs(D, E) and 4s HoMSs-Al$_{0.1}$(F, G)

undoped 4s HoMSs and 4s HoMSs-Al$_{0.1}$, corresponding to the (003) plane of the layered structure[Fig.2(D) and (F)]. Selected area electron diffraction pattern of 4s HoMSs and 4s HoMSs-Al$_{0.1}$ shows polycrystalline electron diffraction rings[Fig.2(F) and (H)]. One of these diffraction rings is indexed to (220) plane of spinel phase, which proves the layered/spinel heterostructure.

3.2.3 XRD, Raman Spectra and XPS

XRD characterization is also carried out to detect the phase purity and crystal structure of the as-prepared LRLO samples. As shown in Fig.3(A), all samples have sharp XRD diffraction peaks, indicating that the material has high crystallinity. Most diffraction peaks can be indexed as an ordered α-NaFeO$_2$ structure(space group is $R\bar{3}m$), while a few peaks between 20°—25° correspond to the Li$_2$MnO$_3$ superlattice structure. In addition, it's worth mentioning that the (003) diffraction peak of the Al-doped material is slightly red shifted[Fig.3(B)], which agrees well with the literatures[14,44].

Raman spectra is shown in Fig.3(C). The scattering peak at 601 cm^{-1} corresponds to the stretching A_{1g} mode of M—O chemical bond(M=Mn, Ni and Co) in the $R\bar{3}m$ layered phase, while the one at 487 cm^{-1} is the E_g vibrational mode signal of the layered phase. There is no obvious difference between the Raman spectra of 4s HoMSs and 4s HoMSs-Al$_{0.1}$, indicating that a small amount of Al doping has little effect on the overall structure. The Raman peak around 422 cm^{-1} is assigned to the monoclinic Li$_2$MnO$_3$ phase, which is consistent with the literature[44].

XPS analysis was adopted to compare the oxidation states of metal ions in LRLO HoMSs before and after Al doping[Fig.3(D)—(F) and Fig.S5]. The peak positions of Mn 2*p*, Ni 2*p* and O 1*s* do not change significantly after doping compared to the undoped one. High-resolution XPS spectra of Mn 2*p* show two main peaks located at 641.9 and 653.6 eV, respectively, corresponding to 2$p_{3/2}$ and 2$p_{1/2}$ states of Mn^{4+}. As for Ni 2*p*, there are two main binding energy peaks of Ni 2$p_{2/3}$ and Ni 2$p_{1/3}$ located at 854.3 and 872.0 eV, in addition to two satellite peaks, which indicates Ni^{2+} dominated in the LRLO HoMS materials. Fig.3(F) presents that binding energy peak of Al 2*p* is located at around 71.0 eV, indicating Al^{3+} in the 4s HoMSs-Al$_{0.1}$.

https://doi.org/10.1007/s40242-023-3128-8

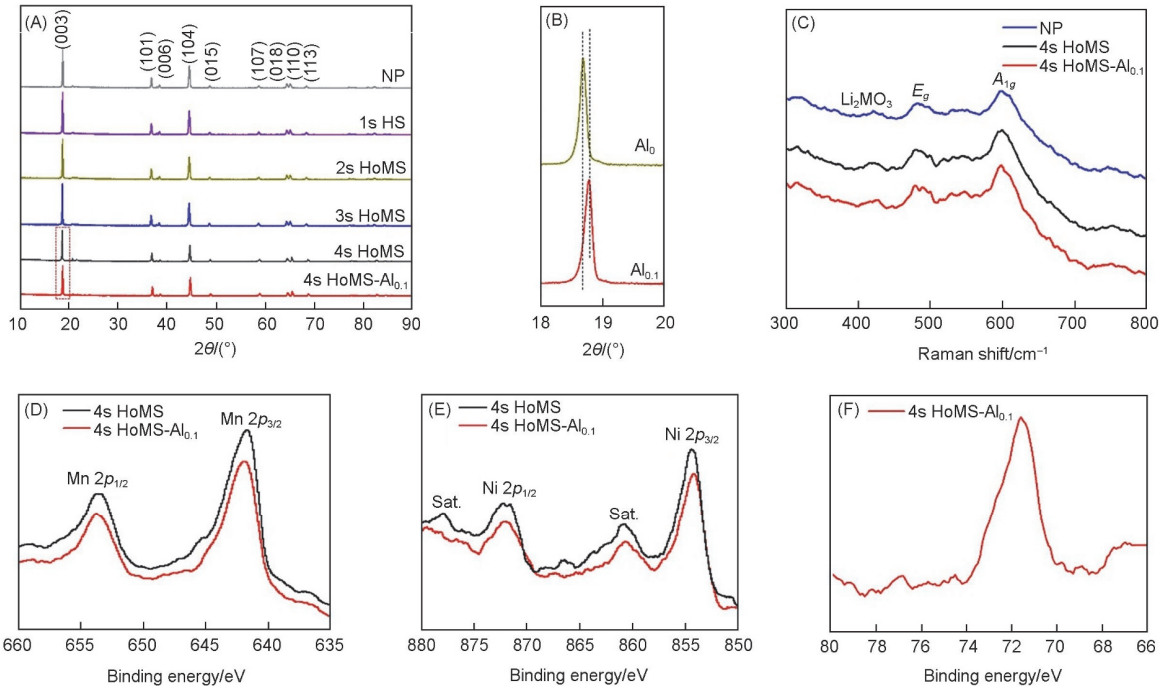

Fig.3 XRD patterns(A), magnified XRD patterns(B), Raman spectra(C), and XPS spectra(D—F) of Mn 2*p*(D), Ni 2*p*(E) and Al 2*p*(F) of Li-rich cathode materials before cycling test

3.3 Electrochemical Performance of LRLO HoMSs

The electrochemical performances of different LRLO HoMS samples are studied by assembling coin cells, tested in a voltage range of 2.0—4.8 V. The charge-discharge voltage profiles of the first cycle tested at 0.1 C(1 C=300 mA/g) are shown in Fig.4(A). During the first charging process, all the prepared LRLO samples exhibit a sloping curve below 4.5 V, corresponding to the redox activity of initially active phase, and a long plateau around 4.5V corresponding to the redox of Li_2MnO_3 phase. The initial discharge capacities of 1s HS, 2s HoMS, 3s HoMS, 4s HoMS, 4s HoMS-$Al_{0.1}$ and nanoparticles are 155.8, 158.8, 211.3, 215.1, 300.6, and 134.5 mA·h·g^{-1}, respectively. It was found that HoMS samples showed a higher discharge capacity than the nanoparticle sample. Besides, the increased shell number benefits the specific capacity, which may be ascribed to that multiple shells could support with each other and the outer shell could protect the inner shell, thus increasing the reversible redox sites. Moreover, Al doping also increase the initial reversible capacity, which may be due to that Al doping enhances reversible oxygen redox, which provides additional capacity.

In order to further study the redox reaction of the material during the delithiation-lithiation process, the differential capacity plots of the first cycle were obtained from the derivation of the charge-discharge curves. As shown in Fig.4(B), the HoMS-based LRLO materials show a similar oxidation peak near 3.8 V, corresponding to the oxidation reaction of Ni^{2+}/Ni^{4+} and Co^{3+}/Co^{4+}, while the oxidation peak in the nanoparticle sample shifts to 3.95 V, which is consistent with the phase occurring in the nanoparticle sample. Another sharp oxidation peak at around 4.5 V corresponds to the activation process of Li_2MnO_3 phase, wherein the peak area of the 4s HoMSs-$Al_{0.1}$ is the largest, indicating that the capacity can be contributed most during the redox process. The main reduction peak is located at around 3.7 V, which belongs to the redox activity of Mn^{4+}/Mn^{3+}. No obvious reduction peak is observed at about 2.5 V for all materials, indicating that no obvious spinel phase transition occurs in the prepared LRLO materials.

Fig.4(C) shows the cycling performance of different LRLO samples performed at 0.5 C. Distinctly, 4s HoMS-$Al_{0.1}$ retains the highest discharge capacity of 246.3 mA·h·g^{-1} after 100 cycles, while those of 1s HS, 2s HoMS, 3s HoMS, 4s HoMS, 4s HoMS-$Al_{0.1}$ are 117.4, 149.4, 166.8, 187.9 and 246.3 mA·h·g^{-1}, respectively. Comparatively, only 99.5 mA·h·g^{-1} remained for LRLO nanoparticles. The higher retained capacity of 4s HoMS-$Al_{0.1}$ could be ascribed to two parts: first, Al doping can stabilize both the surface and bulk of LRLO materials; second, HoMS can effectively buffer the stress/strain during repeated lithiation/delithiation processes, thus further benefiting the structural stability.

The average discharge voltage of each cycle is presented in Fig.4(D). It shows that the average discharge voltage of the 4s HoMSs-$Al_{0.1}$ decreases from 3.81 V to 3.63 V after 100 cycles,

https://doi.org/10.1007/s40242-023-3128-8

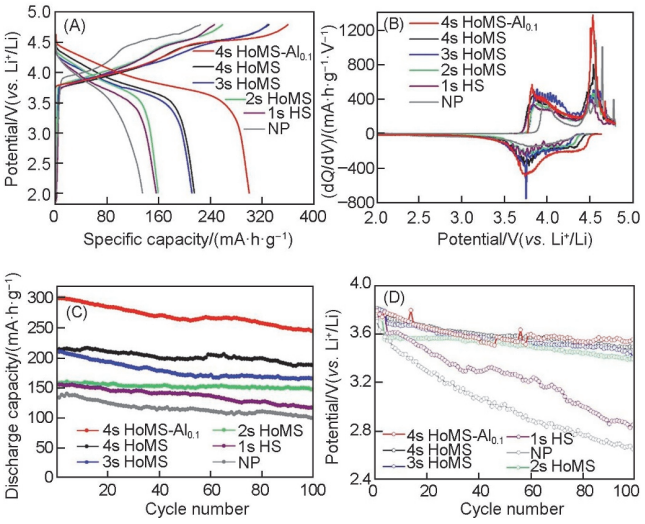

Fig.4 First charge-discharge voltage curves(A), d*Q*/d*V* profiles of the first cycle(B), cycling performance(C), and average discharge potential *versus* cycle number plots of different Li-rich cathode materials(D)

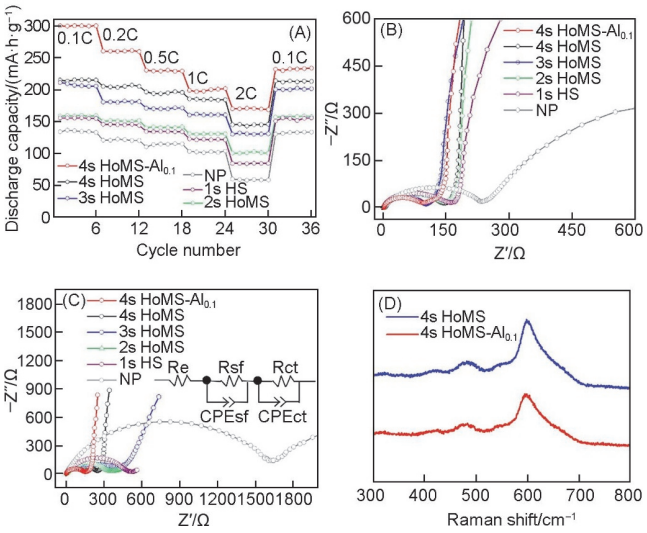

Fig.5 Rate capability(A), electrochemical impedance spectroscopy of different Li-rich cathode materials before(B) and after(C) cycling test, and Raman spectra after cycling test(D)

while that of 4s HoMSs decreased to 3.60 V. On the contrary, the average discharge voltage of the 1s HS and nanoparticle sample decreased from 3.73 and 3.71 V to 3.40 and 3.23 V, respectively. It can be concluded that the HoMSs combined with Al doping significantly help to stabilize the average voltage, which may be due to that the Al doping can restrain the migration of transition metal ions to the lithium ion sites, thereby inhibiting the phase transformations.

Considering that rate capability is also one of the crucial parameters for LIBs, we also conducted charge and discharge tests at different current densities. As shown in Fig.5(A), the discharge specific capacity of 4s HoMSs is higher than those of other materials at every rate. At 2 C, the specific capacities of 4s HoMS-$Al_{0.1}$ and 4s HoMS are about 171.0 and 145.8 mA·h·g^{-1}, while that of the nanoparticle sample is only 59.1 mA·h·g^{-1}. The good rate capability of 4s HoMSs-$Al_{0.1}$ could be ascribed to that thin shells shorten the charge and ion diffusion distance, and the connected multiple shells offer a percolated conductive path to facilitate charge diffusion. In addition, the specific capacity of 4s HoMSs-$Al_{0.1}$ increases back to about 234 mA·h·g^{-1} as the rate decreases to 0.1 C, indicating the reversibility of the structure.

Impedance spectra of different LRLO materials are also compared. Fig.5(B) shows the impedance of cells after the first cycle test. Obviously, the 4s HoMS-$Al_{0.1}$ exhibits a smaller semicircle, indicating that the charge transfer resistance(R_{ct}) of 4s HoMS-$Al_{0.1}$ is smaller than those of 1s HS or nanoparticle samples. In addition, after cycling test, the R_{ct} of nanoparticle samples vigorously increases[Fig.5(C)], indicating that severe interfacial parasitic reactions happened. Comparatively, the increase of R_{ct} for the 4s HoMSs-$Al_{0.1}$ is effectively restrained. This result proves that HoMS combined Al doping strategies could not only significantly decrease charge diffusion resistance but also improve the structure stability and suppress side reactions during cycling. In addition, there is no Raman band corresponding to spinel-like phase after cycling test[Fig.5(D)]. This indicates that Al doped HoMS design effectively suppresses the layered-to-spinel phase transformation, which further supports the good capacity and discharge voltage retention during cycling.

4 Conclusions

Al doped LRLO HoMS is developed through a sequential templating approach with an accurately controlled crystal and geometric structure. Adopted as cathode for LIB, the 4s HoMS-$Al_{0.1}$ sample achieved a high specific capacity, stable voltage and capacity during cycling, exhibiting an initial discharge specific capacity up to 300.6 mA·h·g^{-1} at 0.1 C and maintaining 246.3 mA·h·g^{-1} after 100 cycles. The impressive electrochemical performance is benefited from the synergistic effect of Al doping and HoMS design. HoMS can effectively buffer the stress/strain during cycling, as well as shorten the ion and electron diffusion path, while Al doping can inhibit the phase transition of the material and reduce the surface oxygen precipitation. Our facile strategy for constructing Al doped hollow multishelled structural Li-rich cathodes with high capacity and voltage stability sheds light on developing other high-performance energy storage materials.

Electronic Supplementary Material

Supplementary material is available in the online version of this article at http://dx.doi.org/10.1007/s40242-023-3128-8.

Acknowledgements

This work was supported by the National Key R&D Program of China (Nos.2021YFC2902503, 2022YFA1504101), the National Natural Science Foundation of China(Nos.21820102002, 21931012, 52261160573, 51972305), the Cooperation Fund of the Institute of Clean Energy Innovation, Chinese Academy of Sciences(No.DNL202020), the Zhongke-Yuneng Joint R&D Center Program, China(No.ZKYN2022008), and the IPE Project for Frontier Basic Research, China(No.QYJC-2022-008).

Conflicts of Interest

WANG Dan is an editorial board member for Chemical Research in Chinese Universities and was not involved in the editorial review or the decision to publish this article. The authors declare no conflicts of interest.

References

[1] Park G.-T., Namkoong B., Kim S.-B., Liu J., Yoon C. S., Sun Y.-K., *Nat. Energy,* **2022**, *7*, 946
[2] Yang S., Ai F., Li Z., Zhao G., Bi Y., *Chem. Res. Chinese Universities*, **2021**, *38*(2), 603
[3] Bi Y. J., Tao J., Wu Y., Li L., Xu Y., Hu E., Wu B., Hu J., Wang C., Zhang J. -G., Qi Y., Xiao J., *Science*, **2020**, *370*, 1313
[4] Hou W., Ou Y., Liu K., *Chem. Res. Chinese Universities*, **2022**, *38*(3), 735
[5] Chen W., Xia H., Guo K., Jin W., Du Y., Yan W., Qu G., Zhang J., *Chem. Res. Chinese Universities*, **2022**, *38*(5), 1232
[6] Yin W., Grimaud A., Rousse G., Abakumov A. M., Senyshyn A., Zhang L., Trabesinger S., Iadecola A., Foix D., Giaume D., Tarascon J M., *Nat. Commun.*, **2020**, *11*(1), 1252
[7] House R. A., Maitra U., Perez-Osorio M. A., Lozano J. G., Jin L., Somerville J. W., Duda L. C., Nag A., Walters A., Zhou K. J., Roberts M. R., Bruce P. G., *Nature*, **2020**, *577*(7791), 502
[8] Li Q., Yao Z., Lee E., Xu Y., Thackeray M. M., Wolverton C., Dravid V. P., Wu J., *Nat. Commun.*, **2019**, *10*(1), 1692
[9] Assat G., Tarascon J. M., *Nat. Energy*, **2018**, *3*(5), 373
[10] Seo D. H., Lee J., Urban A., Malik R., Kang S., Ceder G., *Nat. Chem.*, **2016**, *8*(7), 692
[11] Ma Q., Chen Z., Zhong S., Meng J., Lai F., Li Z., Cheng C., Zhang L., Liu T., *Nano Energy*, **2021**, *81,* 105622
[12] Li Q., Li G., Fu C., Luo D., Fan J., Li L., *ACS Appl. Mater. Interfaces*, **2014**, *6*(13), 10330
[13] Choi A., Lim J., Kim H. J., Jung S. C., Lim H. W., Kim H., Kwon M. S., Han Y. K., Oh S. M., Lee K. T., *Adv. Energy Mater.*, **2018**, *8*(11), 1702514
[14] Wang E., Xiao D., Wu T., Liu X., Zhou Y., Wang B., Lin T., Zhang X., Yu H., *Adv. Funct. Mater.*, **2022,** *1616,* 2201744
[15] Luo D., Ding X., Hao X., Xie H., Cui J., Liu P., Yang X., Zhang Z., Guo J., Sun S., Lin Z., *ACS Energy Lett.*, **2021**, *6*(8), 2755
[16] Li Z., Li Y., Zhang M., Yin Z W., Yin L., Xu S., Zuo C., Qi R., Xue H., Hu J., Cao B., Chu M., Zhao W., Ren Y., Xie L., Ren G., Pan F., *Adv. Energy Mater.*, **2021**, *11*(37), 2101962
[17] Wang T., Zhang C., Li S., Shen X., Zhou L., Huang Q., Liang C., Wang Z., Wang X., Wei W., *ACS Appl. Mater. Interfaces*, **2021**, *13*(10), 12159
[18] Yan H., Li B., Yu Z., Chu W., Xia D., *J. Phys. Chem. C*, **2017**, *121*(13), 7155
[19] Wang M. J., Yu F. D., Sun G., Wang J., Zhou J. G., Gu D. M., Wang Z. B., *J. Mater. Chem. A*, **2019**, *7*(14), 8302
[20] Liu J., Wang S., Ding Z., Zhou R., Xia Q., Zhang J., Chen L., Wei W., Wang P., *ACS Appl. Mater. Interfaces*, **2016**, *8*(28), 18008
[21] Wang P., Zhang Z., Song N., An X., Liu J., Feng J., Xi B., Xiong S., *CCS Chem.*, **2023**, *5*(2), 397
[22] Zhao X. Y., Lu Y., Qian Z F., Wang R. H., Guo Z. P., *Ecomat*, **2020**, *2*(3), e12038
[23] Shen L., Song Y. W., Wang J., Zhao C. X., Bi C. X., Sun S. Y., Zhang X. Q., Li B. Q., Zhang Q., *Small Struct.*, **2022,** *7,* 2200205
[24] Wang W., Zhu X., Fu L., *CCS Chem.*, **2021**, *3*(1), 686
[25] Wang Z. S., Wang H. P., Qi S. A., Wu D. X., Huang J. D., Li X., Wang C. Y., Ma J. M., *Ecomat,* **2022***, 4*(2), e12200
[26] Wang J., Cui Y., Wang D., *Adv. Mater.*, **2019**, *31*(38), e1801993
[27] Wang J., Cui Y., Wang D., *Nanoscale Horiz.*, **2020**, *5*(9), 1287
[28] Wang J., Tang H., Ren H., Yu R., Qi J., Mao D., Zhao H., Wang D., *Adv. Sci.*, **2014**, *1*(1), 1400011
[29] Wang L., Wan J., Wang J., Wang D., *Small Struct.*, **2020**, *2*(1), 2000041
[30] Li B., Bi R., Yang M., Gao W., Wang J., *Appl. Surf. Sci.*, **2022**, *56*(3), 586
[31] Ma Y., Bi R., Yang M., Wei P., Qi J., Wang J., Yu R., Wang D., *J. Nanopart. Res.*, **2023**, *25*(1), 14
[32] Wang J., Wang Z., Mao D., Wang D., *Sci. China Chem.*, **2021**, *65*(1), 7
[33] Zhao J., Yang M., Yang N., Wang J., Wang D., *Chem. Res. Chinese Universities*, **2020**, *36*(3), 313
[34] Zhao J. L., Wang J. Y., Bi R. Y., Yang M., Wan J. W., Jiang H. Y., Gu L., Wang D., *Angew. Chem. Int. Ed.*, **2021**, *60*(49), 25719
[35] Wei Y., Wan J., Wang J., Zhang X., Yu R., Yang N., Wang D., *Small,* **2021**, *17*(22), e2005345
[36] Wang J., Wan J., Yang N., Li Q., Wang D., *Nat. Rev. Chem.*, **2020**, *4*(3), 159
[37] Bi R., Mao D., Wang J., Yu R., Wang D., *Acta Chim. Sinica*, **2020**, *78*(11), 1200
[38] Wang J., Tang H., Wang H., Yu R., Wang D., *Mater. Chem. Front.*, **2017**, *1*(3), 414
[39] Wang J., Tang H., Ren H., Yu R., Qi J., Mao D., Zhao H., Wang D., *Adv. Sci.*, **2014,** *1(1),* 1400011
[40] Wei Y., Wang J., Yu R., Wan J., Wang D., *Angew. Chem. Int. Ed.*, **2019**, *58*(5), 1422
[41] Wei Y., Yang N., Huang K., Wan J., You F., Yu R., Feng S., Wang D., *Adv. Mater.*, **2020**, *32*(44), e2002556
[42] Li B., Wang J., Bi R., Yang N., Wan J., Jiang H., Gu L., Du J., Cao A., Gao W., Wang D., *Adv. Mater.*, **2022,** e2200206
[43] Wang J. Y., Yang M., Wang D., *Chin. J. Chem.,* **2022**, *40*, 1190
[44] Nayak P. K., Ginblat J., Levi M., Levi E., Kim S., Choi J. W., Aurbach D., *Adv. Energy Mater.*, **2016**, *6*, 1502398